



Temperature corrections in the Priestley–Taylor equation of evaporation



Jozsef Szilagyi*

Department of Hydraulic and Water Resources Engineering, Budapest University of Technology and Economics, Budapest, Hungary
School of Natural Resources, University of Nebraska-Lincoln, 3310 Holdrege St. HH625, Lincoln, Nebraska, USA

ARTICLE INFO

Article history:

Received 3 June 2014

Received in revised form 12 July 2014

Accepted 19 July 2014

Available online 30 July 2014

This manuscript was handled by

Konstantine P. Georgakakos, Editor-in-Chief

Keywords:

Priestley–Taylor equation

Wet-environment surface temperature

Complementary relationship of evaporation

Evaporation estimation

SUMMARY

The Priestley–Taylor equation (PTE) is frequently applied in actual areal evapotranspiration (ET) estimation methods for obtaining the maximum daily rate of evaporation with data from sub-humid conditions. Since PTE was parameterized under humid conditions, a temperature correction is necessary to avoid overestimation of the maximum rate of ET. Wet-environment surface temperature (T_{ws}), a proxy of the wet-environment air temperature (T_{wa}), is estimated by the Szilagyi–Jozsa (SJ) approach as well as by a re-parameterized version of Monteith. The latter yields higher values but typically within 1 °C of the former. Tested by daily FLUXNET data, the estimates are only mildly sensitive to the mean daily wind velocity which thus can be replaced by a region-representative monthly average. From long-term simplified water-balances – plus monthly Moderate Resolution Imaging Spectroradiometer (MODIS) and ERA-Interim re-analysis data – the re-parameterized Monteith method appears to yield more accurate T_{ws} estimates, while the PTE performs better with the SJ provided T_{ws} values since they are closer to T_{wa} , the PTE expects. Both methods require net radiation, air temperature, humidity and monthly mean wind velocity values plus ground heat fluxes when employed on a daily basis.

Published by Elsevier B.V.

1. Introduction

Since the publication of Priestley and Taylor (1972) describing evaporation of extended wet surfaces under minimal energy advection, the equation they formulated and subsequently became referred to as the Priestley–Taylor equation (PTE), has seen an unprecedented number of applications in hydrology, meteorology, climatology, agronomy, ecology, geology, civil engineering, and their crossbreeds, such as hydrometeorology, ecohydrology, hydrogeology, agricultural meteorology, just to name a few. Google currently lists about 3300 citations to their original article. This number is probably much higher due to early references not included in Google. Indeed, there is hardly any areal evaporation/evapotranspiration (ET) estimation method that would not (at least partially) incorporate the PTE. Even those ET estimation approaches that were developed before the publication of PTE, such as the Thornthwaite and Mather water balance accounting scheme (1955), have been retrofitted with the PTE in many applications (e.g., Sinkevich et al., 2005; Klein, 2013; Szilagyi, 2013a).

The PTE is frequently used to estimate the actual ET rate of wetlands (e.g., Souch et al., 1996; Bidlake, 2000). As the PTE describes the maximum rate of ET that can be achieved at a regional

scale, it is often used as a reference for the estimation of actual areal ET rates in water limited environments as well where soil moisture acts as a limiting factor to evaporation. For example, the soil-moisture function approach obtains actual ET using the PTE, scaled down by a function of the estimated soil moisture (e.g., Davies and Allen, 1973; Spittlehouse and Black, 1981; Chen and Brutsaert, 1995).

In ET estimation methods that are based on the complementary relationship of evaporation (Bouchet, 1963), such as the Advection-Aridity model of Brutsaert and Stricker (1979) and the WREVP model of Morton et al. (1985), actual ET is related to the difference in ET rates of wet surfaces having distinct areal extent (i.e., plot-sized with the corresponding ET rate typically estimated by the Penman equation (1948) or regional, the PTE is in fact valid for).

The PTE is also applied in remote-sensing-based ET estimation approaches. The CREMAP model (Szilagyi, 2013b; Szilagyi and Kovacs, 2010; Szilagyi et al., 2011), a calibration-free method, estimates the actual ET of each ca. 1 km-by-1 km MODIS cell via a combination of the regional ET rate (given by WREVP), and the PTE-obtained value, weighted by the corresponding day-time surface temperature values. The so-called two-source models of remote-sensing based ET estimation approaches (e.g., Anderson et al., 2008; Kustas and Anderson, 2009) rely on the PTE for vegetation canopy ET rate estimates. Another group of remote-sensing based models, the Ts-VI space approach (e.g., Jiang and Islam, 2001; Nishida et al., 2003; Wang et al., 2006), scales the PTE equation with a combination of land-surface temperature and albedo for

* Address: School of Natural Resources, University of Nebraska-Lincoln, 3310 Holdrege St. HH625, Lincoln, Nebraska, USA. Tel.: +1 402 472 9667.

E-mail address: jszilagyi1@unl.edu

obtaining actual ET. Several other, empirical models rely on the PTE via scaling it by a vegetation index (e.g., Anderson and Goulden, 2009; Choudhury, 1994; Kim and Kim, 2008) to yield actual evaporation. See Wang and Dickinson (2012) for an exhaustive review.

The above examples illustrate the wide-spread application of PTE in ET estimation problems for providing a reference (maximum) value of actual regional-scale areal ET rates, and therefore necessitating its correct application. Despite its almost universal presence in evaporation research, little attention has been paid to the fact that the PTE was parameterized under humid conditions (Priestley and Taylor, 1972), over oceans and/or saturated extensive land surfaces and yet it is most often used in sub-humid conditions when the soil is only partially saturated and the corresponding air and surface temperature is higher than what would be observable under full saturation. For example, in the summer time when PTE yields the highest rates, the average daily mean air temperature (T_a) difference between non-irrigated and irrigated areas was found to be about 2.5–3 °C in central California by Lobell and Bonfils (2008) with a corresponding 95% confidence interval of about 2–8 °C, indicating that on individual days this difference can reach 8 °C in California, and 10 °C for Nevada shrubs (Huntington et al., 2011). Therefore employing sub-humid T_a in place of humid-environment T_a , i.e., T_{wa} , in the PTE yields an inflated wet-environment ET rate which then distorts the results of any ET estimation method that employs the PTE.

Below it is demonstrated how the unknown wet-environment surface temperature (T_{ws}) can be estimated from data under drying environmental conditions. The resulting T_{ws} will serve as a proxy for the unknown air temperature over the wet surface (T_{wa}) required by the PTE, since temperature gradients over extensive wet surfaces, the PTE is valid for, are generally mild as latent heat fluxes become more efficient in energy transfer between the wet surface and the ambient air than sensible heat fluxes with the increase of moisture as well as available energy (Q_n) at the surface, thus very efficiently lowering the temperature gradient between the wet surface and the overlying air. For example, numerical experiments of Taylor (1971) for unstable atmospheric stratifications upwind of a dry-to-wet transition in surface water content of the ground, covered with short vegetation, predicted an air temperature inversion up to a distance of about 10 km over the wet surface, eventually reaching a nearly constant temperature profile. Judged from visual extrapolation, Rao et al. (1974) obtained comparable numerical results for similar atmospheric and surface conditions: negligible sensible heat (H) transfer, therefore small vertical temperature gradients at a distance of about 1 km or larger downwind from the dry-to-wet transition. Philip (1987) predicted somewhat larger H values for short vegetation at a distance of 10 km along the wet surface, but the resulting sensible heat flux is still only about 20% of the dry surface value, thus the corresponding vertical temperature gradient is also expected to be reduced by about the same extent.

Unfortunately, measured values are hard to find because the few experiments carried out for investigating the effect of energy advection over irrigated fields lack the size necessary for the PTE (Rider et al., 1963; Dyer and Crawford, 1965). The only exception is of de Vries (1959), where T_{ws} and T_{wa} were measured at a distance of ca. 2 km from the dry-to-wet transition. According to Szilagyi and Schepers (2014), T_{ws} is constant with distance to the dry-to-wet transition downwind the wet surface, therefore plot-scale studies in theory could be used for verifications of the estimated T_{ws} values. However, in the above classical plot-scale experiments T_{ws} is extrapolated from T_{wa} measurements at some distance from the ground [in Rider et al. (1963) it is 5 cm, while in Dyer and Crawford (1965) not specified] with high inherent uncertainty because at this horizontal scale the air-temperature gradient is significant close to the ground due to a highly variable vertical air temperature profile typically exhibiting an inversion

close to the ground. Furthermore, in the Rider et al. (1963) study a spatially constant Q_n is violated due to the presence of tarmac upwind of the wet grass surface, while in Dyer and Crawford (1965) the environmental variables are not published, preventing both studies from further validation purposes.

Below two methods are presented for the estimation of the wet-environment surface temperature, T_{ws} , and the results compared with available measurements. The obtained T_{ws} values then are applied in the PTE for the estimation of ET within a complementary relationship framework to see how they affect the estimates, and validated with eddy-covariance and water-balance data from catchments least disturbed by human activities.

2. Estimation of the wet-environment surface temperature, T_{ws}

2.1. Parameterization of the Penman–Monteith equation

Monteith (1981) derived T_{ws} from air temperature (T_a), specific humidity (q) and net radiation (R_n) data, employing a simplification [similar to the equality of eddy diffusivities for sensible heat (H) and latent heat (LE) in boundary-layer flow (Brutsaert, 1982)] for aerodynamic resistances, r_v and r_H , respectively, of water vapor and sensible heat, i.e., $r_v = r_H = r$. See Appendix A for the step-by-step derivation of the equation

$$T_{ws} = T_a + \frac{rH}{c_p \rho} = T_{wb} + \left(\frac{r(c_p/L)}{c_p \rho (\delta^{wb} + c_p/L)} \right) Q_n \quad (1)$$

where ρ is air density, c_p is the specific heat of air under constant pressure, L is the latent heat of vaporization, and δ^{wb} is the slope of the saturation specific humidity curve at the wet-bulb temperature, T_{wb} . Here $Q_n = R_n - G$ (the last term denoting heat conduction into the soil) is the energy available at the surface for sensible and latent heat fluxes. T_{wb} by definition is obtained via adiabatic cooling, i.e., $H = \rho c_p D_z T_a / r = -LE = -\rho L D_z q / r$, where D_z denotes the vertical difference operator, from which one obtains (see Fig. A1).

$$\frac{c_p(T_{wb} - T_a)}{L[q_s(T_{wb}) - q(T_a)]} = \gamma \frac{T_{wb} - T_a}{e_s(T_{wb}) - e(T_a)} = -1 \quad (2)$$

which is an implicit equation for T_{wb} . Here γ is the psychrometric constant ($=c_p p / 0.622L$, where p is air pressure) and e denotes the actual, while e_s , the saturation vapor pressure. Occasionally (2) would yield T_{wb} values in excess of T_a , due to measurement error. From Fig. A1 T_{wb} can then be approximated in an alternative and explicit way as

$$\frac{c_p(T_a - T_{wb})}{L} \approx \delta(T_a)(T_{wb} - T_a) \quad (3)$$

which upon multiplication by $p/0.622$ and after rearrangement yields

$$T_{wb} \approx \frac{\gamma T_a + T_d \Delta(T_a)}{\gamma + \Delta(T_a)} \quad (4)$$

(e.g., Szilagyi and Schepers, 2014). Here Δ is the slope of the saturation vapor pressure (e_s) curve, and T_d the dew-point temperature.

The corresponding latent heat flux (see Appendix A) has also been specified by Monteith (1965) and became known as the Penman–Monteith equation

$$LE = \frac{\delta^{wb} Q_n + c_p \rho [q_s(T_a) - q(T_a)] / r}{\delta^{wb} + c_p / L} \quad (5)$$

Note that neither (1) nor (5) is yet ready for the practical estimation of T_{ws} because the value of r is not known ‘a priori’. However, r can be parameterized with the help of the Penman equation (1948)

$$LE^{mm} = \frac{\Delta(T_a)}{\Delta(T_a) + \gamma} Q_n^{mm} + \frac{\gamma}{\Delta(T_a) + \gamma} f_u D_e \quad (6)$$

in order to find an explicit expression for the unknown r assuming that Q_n is about the same for a wet surface covered by short vegetation and an open water surface as well as invoking that the two surfaces evaporate at about the same rate (Brutsaert, 1982). Here both LE^{mm} and Q_n^{mm} are given in water depth equivalents of mm d^{-1} , and the Rome wind function, f_u , is defined as $f_u = 0.26(1 + 0.54 u_2)$, u_2 being the mean wind velocity in ms^{-1} , measured at 2-m height above the ground (Brutsaert, 1982), and D_e the vapor pressure deficit [$=e_s(T_a) - e(T_a) = e_s(T_a) - e_s(T_d)$] at T_a .

By equating (5) and (6), r , and thus T_{ws} as well, can be expressed with the help of measured mean wind velocities via the specified wind function. (6) is first transformed into the same flux units (W m^{-2}) as (5) by multiplying it with $c = 28.94 \text{ Wd mm}^{-1} \text{ m}^{-2}$. Then both the numerator and the denominator of (5) is multiplied by $p/0.622$ before equating the results

$$\frac{\Delta^{wb}}{\Delta^{wb} + \gamma} Q_n + \frac{c_p \rho D_e}{r(\Delta^{wb} + \gamma)} = \frac{\Delta(T_a)}{\Delta(T_a) + \gamma} Q_n + \frac{c \gamma f_u D_e}{\Delta(T_a) + \gamma} \quad (7)$$

Rearrangement of (7) yields

$$\begin{aligned} \frac{c_p \rho}{r} &= \frac{\Delta(\Delta^{wb} + \gamma) - \Delta^{wb}(\Delta + \gamma)}{\Delta + \gamma} \frac{Q_n}{D_e} + \frac{c \gamma (\Delta^{wb} + \gamma) f_u}{\Delta + \gamma} \\ &= a \frac{Q_n}{D_e} + b f_u \end{aligned} \quad (8)$$

with a and b defined as

$$a = \frac{\Delta(\Delta^{wb} + \gamma) - \Delta^{wb}(\Delta + \gamma)}{\Delta + \gamma}; \quad b = \frac{c \gamma (\Delta^{wb} + \gamma)}{\Delta + \gamma} \quad (9)$$

Substitution of (8) into (1) finally yields

$$T_{ws} = T_{wb} + \frac{\gamma Q_n D_e}{(\Delta^{wb} + \gamma)(a Q_n + b f_u D_e)} \quad (10)$$

requiring T_a , T_d , Q_n , and u_2 as input, circumventing the specification of r .

2.2. The Szilagyi–Jozsa method

T_{ws} can also be obtained by the consideration that T_{ws} is constant in space (Szilagyi and Jozsa, 2008; Szilagyi and Schepers, 2014) over the wet surface. By assuming that (a) Q_n is about the same over both, the drying and wet surface, and; (b) T_a and $e(T_a)$ remain yet largely unaffected along the plot-sized wet surface, the Bowen-ratio (B_o) for the wet surface can be written as (Szilagyi and Jozsa, 2008)

$$B_o = \frac{H}{LE} \approx \frac{Q_n - LE_p}{LE_p} \approx \gamma \frac{T_{ws} - T_a}{e_s(T_{ws}) - e(T_a)} \quad (11)$$

where LE_p denotes the Penman-evaporation rate of (6). As (2), (11) is also an implicit equation, but for T_{ws} , to be solved through iterations. It requires the same input variables as (10).

Note that the wet-surface temperature of (10) and (11) may be smaller or larger than T_a , measured at a certain height above the ground, depending on how close the air is to saturation and how large is net radiation. In arid, semi-arid regions T_{ws} is typically less than T_a . The difference increases with aridity and air temperature, and may reach (or exceed, as seen later) 10°C (Huntington et al., 2011).

3. Testing estimates of the wet-environment surface temperature

With the help of FLUXNET data from the 2000–2001 period, estimates of T_{ws} (Fig. 1) were compared for a semi-arid savanna station, about 4 km south of the Okavango delta near the city of Maun in Botswana, located at latitude -19.92° and longitude 23.56° . The elevation is 950 m above sea level, with mean annual precipitation (P) of 460 mm and temperature of 22°C . The location is ideal for studying the behavior of the T_{ws} estimates under radiation, temperature and aridity extremes before and after the wet season. With the exception of a brief period, the two T_{ws} estimates are close to each other, (10) yielding typically larger values than (11) but staying within about 1°C (Fig. 2). When this was not the case (between days 270 and 290), at the start of the wet-season of 2001, measurement error is suspected, since with the obvious increase in humidity by the arrival of rains, the corresponding dew-point temperature values fell to all-time minima, below -20°C (Fig. 2). This could most probably be caused by a severe underestimation of the actual water vapor content (due e.g., to a malfunctioning hygrometer).

As expected, T_{ws} (the arithmetic mean of the two T_{ws} estimates) stays below T_a most of the time, occasionally by more than 10°C (Fig. 2), but on average only 3.5°C lower than T_a (Table 1). This is in accordance with the findings of Lobell and Bonfils (2008) of a $2.5\text{--}3^\circ\text{C}$ mean daily air temperature difference between extensive irrigated and non-irrigated land areas in California. By accepting equilibrium profiles and a 1°C difference between T_{ws} and T_{wa} over the wet areas of the Okavango, according to Ortman (2009) who reports that water temperatures stay within 1°C of air temperatures (although not specifying which one is larger), one obtains a difference of $2.5\text{--}4.5^\circ\text{C}$ in air temperatures between dry and wet areas, which overlaps with the results of Lobell and Bonfils (2008) and a possible larger difference also appears realistic in light of the larger R_n values in Botswana.

As seen in Figs. 1 and 2, T_{ws} may occasionally be larger than the corresponding T_a value. It always happens when humidity of the air increases, marked by local maxima of T_d in Fig. 2, typically on days with rain, although the measured amount may not be significant enough to show up in the precipitation record. When the air is humid, point 1 in Fig. A1 slides closer to point 2 along the adiabatic line, thus making it possible for T_{ws} to be larger than T_a , for the same Q_n .

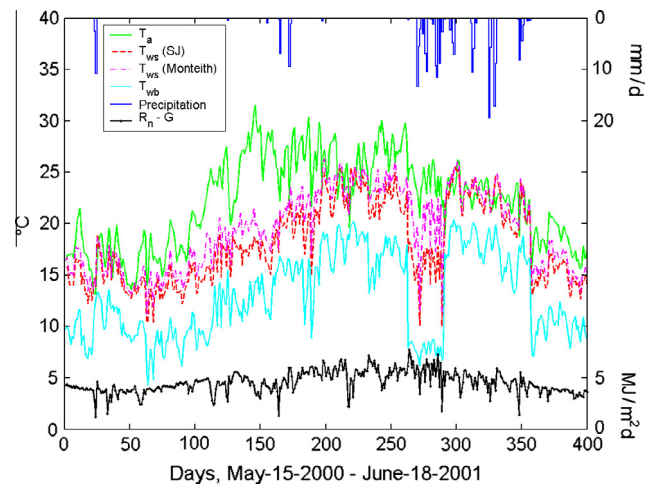


Fig. 1. Measured daily precipitation, available energy at the surface for latent and sensible heat fluxes ($R_n - G$), mean daily air temperature (T_a), as well as estimated wet-bulb (T_{wb}) and wet-surface temperatures by (10, T_{ws}^M) and (11, T_{ws}^J).

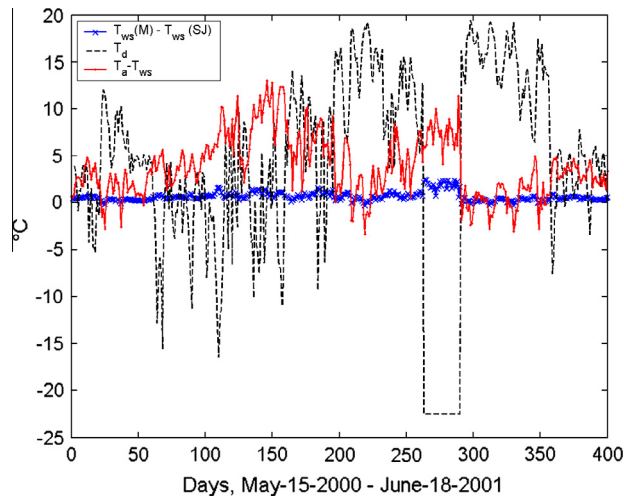


Fig. 2. Differences in the T_{ws} values of (10, M) and (11, SJ) as well as in T_a and the arithmetic average of the two T_{ws} estimates. The corresponding T_d values are also displayed, calculated from published D_e values of FLUXNET.

A potentially useful property of the T_{ws} estimates is their relatively low level of sensitivity to actual wind velocities. Fig. 3 displays differences in the T_{ws} estimates as a response to switching from mean daily wind velocities to 30-day averaged values. Standard deviation is 0.59 °C for (10) and 0.48 °C for (11). Historically, daily wind velocities are harder to obtain than temperature values, therefore the daily T_{ws} estimates can still be obtained from mean monthly values of wind velocities not necessarily from the same station but from one that is representative of the region.

4. Validation of the wet-environment surface temperature estimates

Unfortunately, direct validation of the T_{ws} estimates is not straightforward because measured T_{ws} values are surprisingly scarce not only for the nearby Okavango delta, but in general. Since the average water depth in the delta is less than 1 m (Wolski and Murray-Hudson, 2005), water temperature could serve as a proxy for T_{ws} . Cawley et al. (2012) reported daytime water temperatures of about 18 °C for August of 2010. Mean air temperature was 21.2 °C for the same month with no precipitation (source: weatherspark.com). Since radiation data is not available for 2010, it is not possible to estimate the corresponding T_{ws} . A potential rudimentary check of what this temperature might have been is by taking consecutive moving averages of the 2000 T_a and T_{ws} values over a 31-day period between days 50 and 150 in Fig. 1, and stopping when the average T_a equals about 21.2 °C. The resulting daily mean T_{ws} values are 16.62 [from (10)] and 15 °C [from (11)], respectively, which are 1.38 and 3 °C less than the measured daytime water temperature, suggesting that none of the daily estimates are physically impossible.

Another direct validation possibility of the T_{ws} estimates comes from the unique large-scale study of de Vries (1959) near Rochester, Victoria in Australia on local advection effects over a

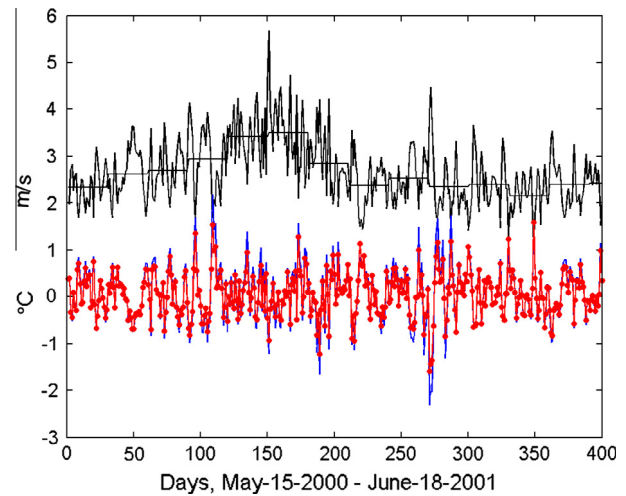


Fig. 3. Differences in the T_{ws} estimates (red dots: T_{ws}^S) caused by a switch from mean daily wind velocities to 30-day averages (upper black lines), measured at 12.6 m above the ground. (For interpretation of the references to colour in this figure legend, the reader is referred to the web version of this article.)

moisture/temperature jump of the land surface in the form of an irrigated field within a dry environment and also contains the necessary data, as average daily mean values over a two-week irrigation period, for the application of (10) and (11). Besides the non-irrigated station upwind, there were three stations located roughly 1, 2, and 3 km downwind from the dry-to-wet transition, denoted as stations 1, 2, and 3. The area was heavily irrigated on day one, with little rain occurring throughout the rest of the experiment. Daily mean T_a over the non-irrigated land was 22.1 °C, while it was 20.7, 20, and 19.7 °C at the three irrigated stations at increasing distance from the dry-to-wet transition, indicating that the air-temperature profile has not reached its equilibrium state at station 2, where T_{ws} estimates could be obtained as measured soil temperature at a depth of 5 cm corrected by the soil temperature gradient for obtaining an estimated surface value of 18.7 °C. The corresponding T_{ws} estimates of (10) and (11) are 19.6 and 18.8 °C, respectively, both of them within 1 °C of the 'observed' value. As de Vries (1959) discusses, the true T_{ws} value must be somewhat larger than 18.7 °C due to the shading effect of the dense irrigated grass cover.

As the publication date of the de Vries' study indicates, mean daily surface temperature, unlike other standard meteorological data, such as temperature and humidity, is not a readily available variable. Even with the help of remote sensing, one typically finds instantaneous surface temperature values, as the case with Moderate Resolution Imaging Spectroradiometer (MODIS) data (modis.gsfc.nasa.gov), in place of a temporal (e.g., daily) average. In the other hand, re-analysis data, such as the 0.7°-resolution ERA-Interim data (apps.ecmwf.int/datasets/) of the European Centre for Medium-Range Weather Forecasts (ECMWF), do include temporal averages, among them mean daily modeled T_s values. For mean daily T_a and T_d value grids over the US, the PRISM data set (prism.oregonstate.edu) is considered the most accurate source.

Table 1
Measured/estimated values of atmospheric and radiation variables for the FLUXNET site near Maun, Botswana (May 15, 2000 – June 18, 2001). T_{ws} is the arithmetic mean of T_{ws}^M by (10) and T_{ws}^S by (11).

	T_a (°C)	T_{wb} (°C)	T_{ws}^S (°C)	T_{ws}^M (°C)	T_{ws} (°C)	P (mm d ⁻¹)	$R_n - G$ (W m ⁻²)	u (ms ⁻¹)	D_e (hPa)
Max	31.53	20.37	25.56	26.29	25.93	19.5	223	5.98	40
Min	13.1	4.27	9.97	11.2	10.59	0	34	1.14	1.01
Mean	22.15	12.87	18	19.3	18.65	0.53	131	2.68	17.74

Net radiation is another variable, not readily available, but obtainable as the sum of the ERA-Interim H and LE values (assuming soil heat conduction is negligible for periods of a day or longer) and also estimated by the WREVP program of Morton et al. (1985) with global radiation input from NOAA (atmos.umd.edu/~srb/gcip/cgi-bin/historic.cgi). Wind data is available from the National Climatic Data Center's (ncdc.noaa.gov) automated surface observation weather station network. Because daily mean T_s is a modeled data by ERA-Interim, and no routine observation exists of the land surface temperature, it is probably best to make a comparison with the present T_{ws} estimates on a monthly basis. Monthly averaging reduces the uncertainty of the modeled daily T_s (and also Q_n) values, thus greatly improving the validation of the T_{ws} estimates, since any discrepancy of the two values then can be attributed to errors in the estimates and not simultaneously to errors in the ERA-Interim modeled values, assuming the latter is an unbiased estimate of the true T_s values.

Szilagyi and Schepers (2014) recently demonstrated the invariance of T_{ws} to changes in aridity provided Q_n and wind conditions stay largely unchanged as the environment dries from a previous wet state. From (1) it follows that T_{wb} stays constant (Q_n and r assumed constant) as long as T_{ws} does, since the change in air density with normal air temperature variations is negligible. Altogether 20 ERA-Interim cells cover central Nebraska, chosen due to its great contrast in aridity, having dry and hot air in the rangelands of the Sand Hills in July, while cooler and more humid air over the extensively irrigated croplands east and southeast of it, July being the prime month for irrigation within Nebraska. From the 10-year period of 2000–2009, altogether 59 ERA-Interim cells were chosen with Q_n from the range [$143 - 2.86 \text{ W m}^{-2}$; $143 + 2.86 \text{ W m}^{-2}$] and the corresponding T_a , T_d , T_{wb} , and estimated T_{ws} values plotted (Fig. 4) against MODIS daytime surface temperature, T_{sd} , as an indicator of aridity. As theory [(1) and Fig. A1] predicts, the wet-bulb and wet-surface temperatures stay constant as the environment dries adiabatically under quasi-constant wind (and Q_n) conditions, marked by opposite changes in air and dew-point temperatures as aridity increases. To validate the two T_{ws} estimates, scattered around $22 \text{ }^\circ\text{C}$ (from 10) and $21.37 \text{ }^\circ\text{C}$ (from

11), both with a standard deviation, s_d , of $0.76 \text{ }^\circ\text{C}$, one must obtain the T_s value under wet environmental conditions. This happens when the air becomes close to saturation over the extensive wet surface, meaning that at saturation T_a (and T_d) must approximate the temporally quasi-constant T_{wb} value of $18.8 \text{ }^\circ\text{C}$ obtained by (4). With the ERA-Interim T_s and PRISM T_a values one can derive the corresponding T_{ws} value by relating the two via the arithmetic average of the two first-order polynomials of Fig. 5. It is recommended to do so (even though this way one does not employ a best-fit equation in the classical sense) in order to be able to use the same transformation equation and to avoid having different (T_s , T_a) pairs depending on which value one starts with to obtain the other. Note that the $T_s \approx T_a + 3.2$ relationship of Fig. 5 is somewhat unrealistic because a decreasing temperature difference is expected between the surface and the air with colder temperatures. This is assured by $T_s = 1.185T_a - 1.25$, which is the arithmetic average of the two best-fit equations, written now for T_s . Under the specified conditions (Q_n and wind) and with $T_{wb} = 18.8$, T_{ws} becomes $21 \text{ }^\circ\text{C}$ with an s_d of about $0.9 \text{ }^\circ\text{C}$ [i.e., $\approx (1 - r_c^2)^{0.5} s_d(T_s) = 1.72(1 - 0.86^2)^{0.5}$]. The s_d intervals (i.e., $0.76 \text{ }^\circ\text{C}$) of both T_{ws} estimates (22 and $21.37 \text{ }^\circ\text{C}$) overlap with the uncertainty-interval of the derived $T_{ws} = 21 \text{ }^\circ\text{C}$.

In reality however, the air temperature is always higher than T_{wb} even over extensive wet surfaces, due to sensible heat transport from the wet surface into the air as well as to entrainment of free tropospheric air into the convective boundary layer, reflected in the larger than unity value of the parameter, α , in the Priestley–Taylor equation (Priestley and Taylor, 1972).

$$LE_w = \alpha \frac{\Delta(T_{wa})}{\Delta(T_{wa}) + \gamma} Q_n \quad (12)$$

where LE_w is the wet-environment ET rate. An $\alpha > 1$ [typically within the range of 1.2–1.32, see Brutsaert (1982) for calibrated α values of different authors] signifies that full saturation does not occur, large-scale convection mixes drier and warmer air over the wet surface, elevating the air temperature and preventing its saturation at the same time. Provided this large-scale convection works similar to local-scale advection, then T_{ws} would not be affected. This way T_{wa} in (12) can be expected to fall within T_{wb} and T_{ws} .

One can, of course, regress the ERA-Interim T_s value against MODIS T_{sd} , ($T_s = 0.286 T_{sd} + 17.4$, with $r_c = 0.66$) to find the smallest

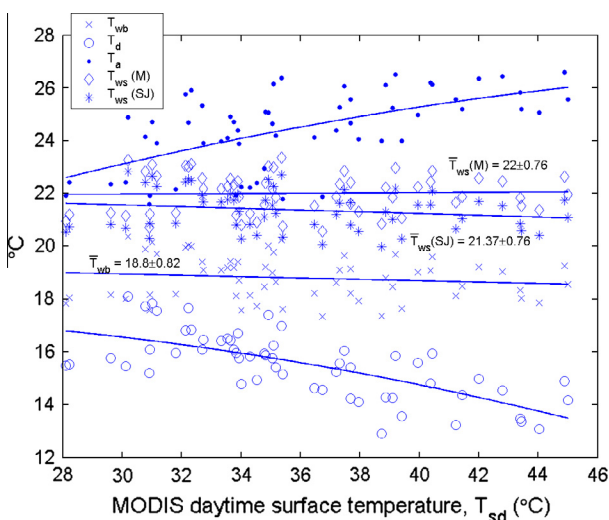


Fig. 4. PRISM-derived mean daily T_a and T_d values in July (2000–2009) as a function of MODIS-derived daytime surface temperature (T_{sd}), both aggregated to 0.7° ERA-Interim cells of central Nebraska having $Q_n = 143 \pm 2.86 \text{ W m}^{-2}$ to ensure a spatially quasi-constant energy available at the surface. The straight lines are the near-constant best fitting first-, while the curves, second-order polynomials of coefficient values $(-0.0045; 0.53; 11.24)$ for T_a , and $(-0.0049; 0.16; 16.14)$ for T_d , both in decreasing power order. The overbar denotes the sample mean ($n = 59$) with the corresponding standard deviation.

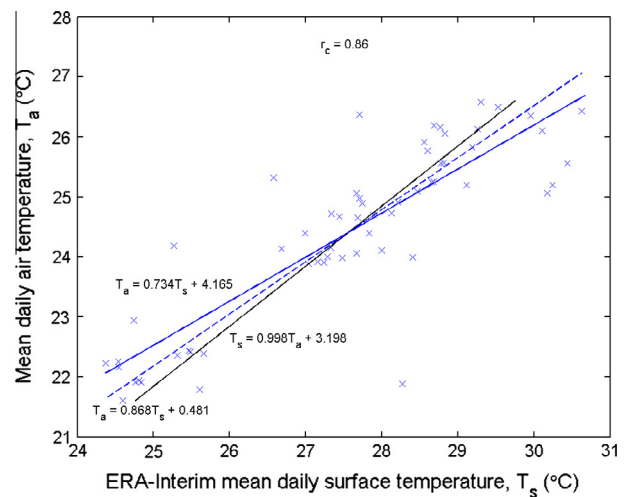


Fig. 5. Regression plot of PRISM mean daily T_a against ERA-Interim mean daily T_s values ($n = 59$) for cells with $Q_n = 143 \pm 2.86 \text{ W m}^{-2}$ in the months of July, 2000–2009 over central Nebraska. The two solid lines are the best fit first-order polynomials [$T_a(T_s)$ and $T_s(T_a)$], the intermittent line their arithmetic average. The correlation coefficient, r_c , is 0.86. $\bar{T}_s = 27.56 \pm 1.72 \text{ }^\circ\text{C}$; $\bar{T}_a = 24.41 \pm 1.47 \text{ }^\circ\text{C}$.

T_s value in the hope that it would correspond to fully wet conditions. The T_{ws} value that corresponds to the coldest observed ca. 1 km MODIS cell value of $T_{sd} = 24.21$ °C in July, this way becomes 24.32 ± 1.29 °C, indicating that the cell-surface has not reached fully wet conditions. The corresponding T_a value via extrapolation from Fig. 4 is 21.45 ± 1.19 °C, while Fig. 5 (via the intermittent line) yields 21.59 ± 0.75 °C for the coldest MODIS cell. For comparison, the coldest 4 km PRISM T_a value is 21.6 °C, corroborating (through the correctly estimated T_a values) the validity of the T_{ws} estimate for the coldest MODIS cell, which thus has not reached a fully wet state.

All this is in agreement with Szilagyi et al. (2011) who used the coldest MODIS pixel values over large wet or open water areas to obtain corresponding ET rates, described by the Priestley–Taylor equation. These coldest cells typically coincide with wetlands, shallow lakes or reservoirs since irrigated center-pivot areas in Nebraska have a typical diameter of 7–800 m (Szilagyi and Schepers, 2014), thus are unable to completely fill a MODIS cell, leaving unirrigated areas in each cell and that way preventing MODIS to detect full saturation over them. The selected ERA-Interim cells with $Q_n = 143 \pm 2.86$ $W\ m^{-2}$ within Central Nebraska apparently do not include any of these extended wet areas.

Szilagyi and Jozsa (2008), Szilagyi et al. (2009), Huntington et al. (2011) and McMahon et al. (2013) employed T_{ws} of (11) for the approximation of T_{wa} . Below the same approach is followed by making use of the T_{ws} estimates of (10) and (11) and employing a Priestley–Taylor parameter value from the typical [1.2–1.32] interval. Note that the interval corresponds to a ca. 5% change in the accepted mean value of $\alpha = 1.26$ (Priestley and Taylor, 1972). Note also that the goal is not a calibration of α since in most cases it cannot be implemented in practice due to a lack of measured ET rates. The aim here rather is to see which T_{ws} estimate performs better with α values taken from the well-accepted interval of [1.2–1.32] in order to be able to recommend one over the other based on their performance in these tests. Ideally, the better performing T_{ws} value could be used in future studies with $\alpha = 1.26$ (as was done in Huntington et al., 2011), thus obviating calibration, but it, as seen below, would be sub-optimal probably in most applications. Nevertheless, as seen below, a mere 5% change in the value of α , in combination with the estimated T_{ws} values, is sufficient to achieve acceptable ET estimates.

5. Application of T_{ws} for ET estimation by the modified Advection-Aridity model

Szilagyi and Jozsa (2008) modified the Advection-Aridity model of Brutsaert and Stricker (1979) which is based on Bouchet's (1963) complementary relationship (CR) of evaporation, to estimate actual ET by accounting for the change in air temperature between drying (T_a) and wet (T_{wa}) surfaces, i.e.,

$$LE^{mm} = 2LE_w^{mm} - LE_p^{mm} = \left[\frac{2\alpha\Delta(T_{wa})}{\Delta(T_{wa}) + \gamma} - \frac{\Delta(T_a)}{\Delta(T_a) + \gamma} \right] Q_n^{mm} - \frac{\gamma}{\Delta(T_a) + \gamma} f_u D_e \quad (13)$$

where T_{wa} was approximated by T_{ws} of (11), Q_n and all ET rates are expressed in $mm\ d^{-1}$. Note that (12) was derived under wet-environmental conditions, yet in practice it is most often applied in (13) with data taken over drying land surfaces, i.e., T_{wa} is substituted by actual T_a . As seen in Fig. 2, the difference in the two values may reach 12 °C in a hot and arid environment, therefore the difference in the $2\Delta/(\Delta + \gamma)$ term can be significant between T_a and T_{wa} . With $T_a \approx 31$ °C from Fig. 1 and $T_{wa} \approx 19$ °C from Fig. 2, the corresponding values are 1.62 and 1.4, a ca. 14% difference, which is almost three times the range typically accepted for the value of α .

Actual ET via (13), with the T_{ws} estimates of (10) and (11) is first estimated for the Botswana FLUXNET site over the available full period of February 1, 1999 – October 31, 2001. The 31 days in Fig. 2, when T_a fell below -20 °C were left out of the analysis. As Fig. 6 demonstrates, the energy balance is not closed, there is a significant underestimation of, both H and LE fluxes, not uncommon with eddy-covariance measurements, where a 20% underestimation is routinely reported (Wang and Dickinson, 2012). Admittedly, energy closure is a far more complex task than a simple correction through polynomial fitting, yet it was performed here in lack of the original raw measurements. The correction involved adding the residuals of the 2nd-order polynomial fit to Q_n , by assuming that underestimation evenly affected both fluxes. Application of (13) with the most commonly accepted value of $\alpha (=1.26)$ resulted in overestimations of 51% when $T_{wa} = T_a$ is applied (original AA model), 29% via (10), and 23% via (11) of the mean daily ET value of 1.37 mm. With $\alpha = 1.2$, these overestimations reduce to 28, 9, and 4%, respectively. See Fig. 7 for the results of the latter case, displaying monthly aggregates. It should be noted that the T_a to T_{ws}

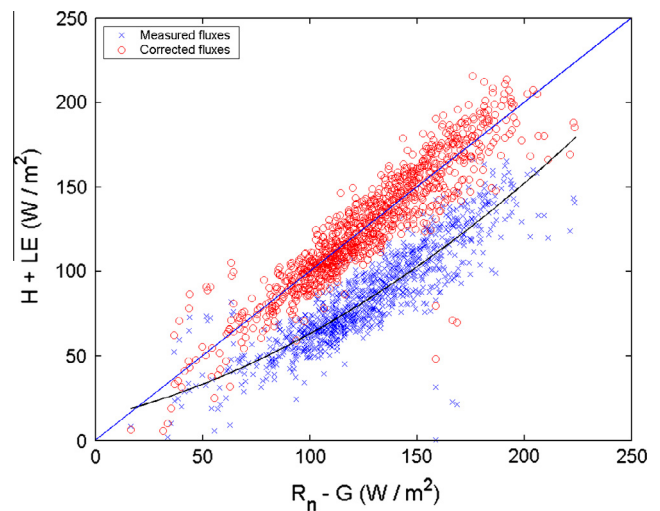


Fig. 6. Test of energy closure for the measured fluxes (02-01-1999 – 10-31-2001) at the FLUXNET site near Maun, Botswana. Coefficient values (in decreasing power order) of the 2nd-order best-fit polynomial: 1.63; 8.71; 13.26. Corrected fluxes are the sum of $Q_n (=R_n - G)$ plus the residuals of the polynomial fitting.

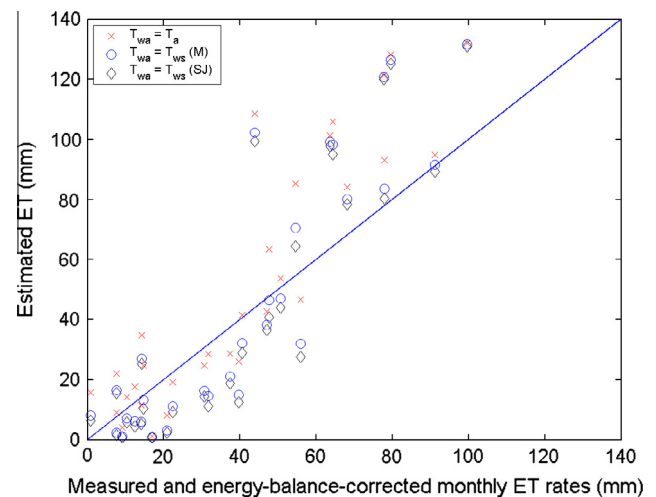


Fig. 7. Monthly-aggregated daily ET estimates of (13) with $\alpha = 1.2$, plotted against energy-balance-corrected measured values (02-01-1999 – 10-31-2001) at the FLUXNET site near Maun, Botswana. $r_c \approx 0.9$ for all three estimates.

correction is only meaningful when T_{ws} is actually smaller than T_a . In relatively humid days T_{ws} can indeed become larger (Fig. A1) than T_a (although not the true T_{wa} value the T_{ws} estimate is a proxy of), thus in such days the correction is meaningless, therefore in these days T_{ws} is capped by T_a (Szilagyi and Jozsa, 2008; Huntington et al., 2011; McMahon et al., 2013). Also, (13) expects wind velocities measured at 2 m above the ground. However, the FLUXNET station is in the middle of a relatively dense savanna forest, wind being measured at 12.6 m above the ground, thus at an unknown distance above the canopy. Therefore no conversion of the wind velocity values to 2 m was attempted. The original AA model (i.e., $T_{wa} = T_a$) performs worse in the driest and in moderately wet months (overshoots), while it performs better in months of average wetness in comparison with the modified model. All three models overshoot ET rates in wet months, performing the same in the wettest month, since then T_{wa} indeed equals or very near to T_a in all of them.

Performance of (13) was further tested with long-term (30 years) simplified water balances (i.e., ET equals precipitation less runoff) of 25 US catchments, only minimally affected by human influences within the 1961–1990 time period. See Szilagyi et al. (2009) for a spatial distribution of the watersheds. Over a 30-year period, differences in groundwater levels (in the absence of long-term trends) and in soil moisture status between the starting and ending days is negligible in comparison to the accumulated in- and outgoing water fluxes of the catchments, enabling an accurate estimation of watershed-representative ET. See Szilagyi et al. (2009) for meteorological and hydrological data sources. Fig. 8a depicts the mean annual ET estimates of (13) with $\alpha = 1.26$, regressed against water-balance ET rates, with a sample mean of 698 mm yr^{-1} . All models underestimate the sample mean by 6%, 6%, and 10%, in the order of the figure legend. With $\alpha = 1.32$ (panel b), (13) with (11) is right on target, while the other two overestimate ET by 4%. In all cases considered, $r_c \approx 0.96$, signifying

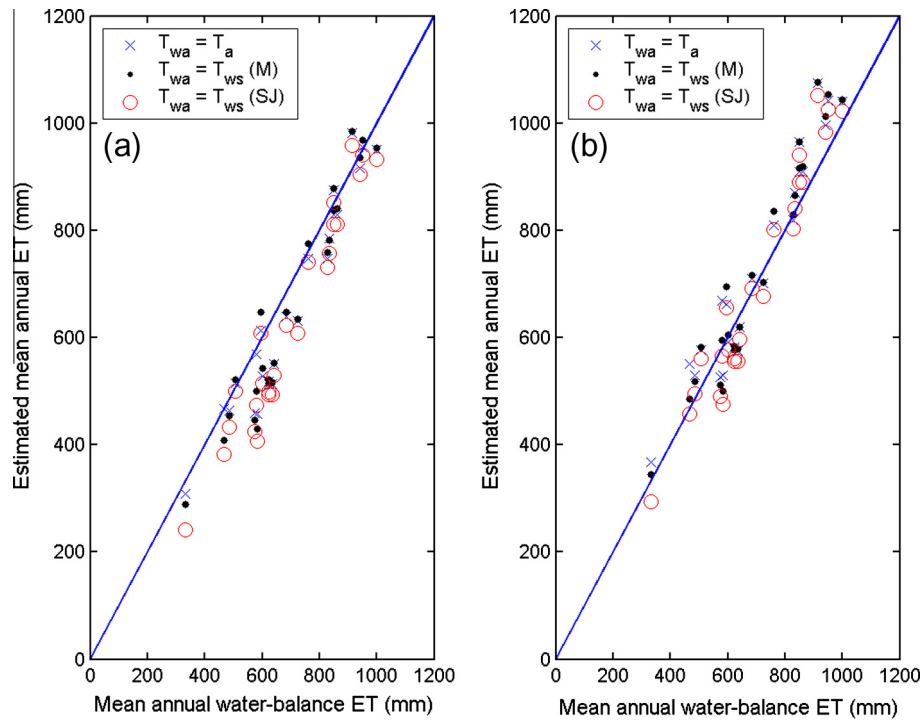


Fig. 8. Long-term (1961–1990) mean annual ET estimates of (13) for 25 minimally altered US catchments with (a) $\alpha = 1.26$; (b) $\alpha = 1.32$. Sample mean of water-balance ET is 698 mm yr^{-1} , $r_c \approx 0.96$ for all three estimates.

Table 2
Validation summary of the estimated T_{ws} values and their performance in ET estimation. std denotes standard deviation.

Site	Measured/assessed T_{ws} or T_{wd} (°C)	Estimated T_{ws} ; std of T_{ws} change due to a switch of daily to monthly wind values (in parenthesis) (°C)		Mean relative error (%) in CR ET estimates using $T_{wa} \approx T_{ws}$ of (10) or (11), or $T_{wa} \approx T_a$	
		(10, M)	(11, SJ)		
FLUXNET site near Maun, Botswana (02-01-99 – 10-31-01)	$T_{wd} = 18$ Cawley et al. (2012)	16.62 (0.59)	15 (0.48)	$\alpha = 1.26$ (T_a): 51 (10): 29 (11): 23	$\alpha = 1.2$ 28 9 4
Irrigation district, Victoria, Australia (12-08-57 – 12-22-57)	$T_{ws} = 18.7$ de Vries (1959)	19.6	18.8		
Central Nebraska, US (2000–2009)	$T_{ws} = 21 \pm 0.9$	22 ± 0.76	21.37 ± 0.76		
Continental US, 25 minimally altered catchments (1961–1990)	–	–	–	$\alpha = 1.26$ (T_a): –6 (10): –6 (11): –10	$\alpha = 1.32$ 4 4 0

by which one obtains

$$q_s(T_{ws}) - q_s(T_{wb}) \approx \frac{\delta^{wb}}{\delta^{wb} + c_p/L} \frac{rQ_n}{\rho L} \quad (\text{A7})$$

From (A1) and (A7) (see Fig. A1) the evaporation rate of the wet surface having a temperature T_{ws} under $Q_n > 0$ is given by

$$\begin{aligned} LE &\approx \frac{\rho L D_z q}{r} = \frac{\rho L}{r} \left[\frac{\delta^{wb}}{\delta^{wb} + c_p/L} \frac{rQ_n}{\rho L} + \frac{c_p(T_a - T_{wb})}{L} \right] \\ &= \frac{\delta^{wb}}{\delta^{wb} + c_p/L} Q_n + \frac{c_p \rho (T_a - T_{wb})}{r} \end{aligned} \quad (\text{A8})$$

thus the corresponding sensible heat flux becomes

$$\begin{aligned} H &\approx \left(1 - \frac{\delta^{wb}}{\delta^{wb} + c_p/L} \right) Q_n - \frac{c_p \rho (T_a - T_{wb})}{r} \\ &= \left(\frac{c_p/L}{\delta^{wb} + c_p/L} \right) Q_n - \frac{c_p \rho (T_a - T_{wb})}{r} \end{aligned} \quad (\text{A9})$$

From (A1) the same H can be written as

$$H = \frac{c_p \rho (T_{ws} - T_a)}{r} \quad (\text{A10})$$

therefore, by combining (A9) and (A10), one obtains (1). Finally, insertion of (A5) into (A8) yields the well-known Penman–Monteith Eq. (5).

Note that this derivation of Monteith (1981) of the temperature and heat fluxes of a wet surface is zero-dimensional, thus the derived fluxes of (A8) and (A9) [with the corresponding T_{ws} of (1)] are not a function of the distance taken downwind from the dry-to-wet transition in surface soil moisture. A recent study of Szilagyi and Schepers (2014), however, supported the constancy of Q_n and thus T_{ws} along the entire (even in the vicinity of the moisture transition) wet homogeneous surface with short vegetation, making (1) [but not 5, 8 or 9, as the fluxes are not constant along the wet surface] powerful for describing the wet surface temperature. Note also that the derived fluxes are valid only for plot-sized areas, as the derivation made explicit use of the assumption that T_a and $q(T_a)$ are not affected significantly by the presence of the wet surface. As the size of the wet area increases, it will affect both the temperature as well as the moisture content of the overlying air significantly, thus the Penman–Monteith Eq. (5) [also (A8), (A9)], cannot be used for such extensive surfaces.

References

- Anderson, R.G., Goulden, M.L., 2009. A mobile platform to constrain regional estimates of evapotranspiration. *Agric. Forest Meteorol.* 149 (5), 771–782.
- Anderson, M.C., Norman, J.M., Kustas, W.P., Houborg, R., Starks, P.J., Agam, N., 2008. A thermal-based remote sensing technique for routine mapping of land-surface carbon, water and energy fluxes from field to regional scales. *Remote Sens. Environ.* 112 (12), 4227–4241.
- Bidlake, W.R., 2000. Evapotranspiration from a bulrush-dominated wetland in the Klamath Basin, Oregon. *J. Am. Water Res. Assoc.* 36, 1309–1320.
- Bouchet, R.J., 1963. Evapotranspiration reelle, evapotranspiration potentielle, et production agricole. *Annal. Agronom.* 14, 743–824.
- Brutsaert, W., 1982. Evaporation into the Atmosphere: Theory, History and Applications. D. Reidel, Dordrecht, Holland.
- Brutsaert, W., Stricker, H., 1979. An advection-aridity approach to estimate actual regional evapotranspiration. *Water Resour. Res.* 15, 443–449.
- Cawley, K.M., Wolski, P., Mladenov, N., Jaffe, R., 2012. Dissolved organic matter biogeochemistry along a transect of the Okavango Delta, Botswana. *Wetlands* 32, 475–486.
- Chen, D., Brutsaert, W., 1995. Diagnostics of land surface spatial variability and water vapor flux. *J. Geophys. Res.* 100 (D12), 25595–25606.
- Choudhury, B.J., 1994. Synergism of multispectral satellite observations for estimating regional land-surface evaporation. *Remote Sens. Environ.* 49 (3), 264–274.
- Cristea, N.C., Kampf, S.K., Burges, S.J., 2013. Revised coefficients for Priestley–Taylor and Makkink–Hansen equations for estimating daily reference evapotranspiration. *J. Hydrol. Eng.* 18 (10), 1289–1300.
- Davies, J.A., Allen, C.D., 1973. Equilibrium, potential, and actual evaporation from cropped surfaces in southern Ontario. *J. Appl. Meteorol.* 12, 647–657.
- de Vries, D.A., 1959. The influence of irrigation on the energy balance and the climate near the ground. *J. Meteorol.* 16, 256–270.
- Ding, R., Kang, S., Li, F., Zhang, Y., Tong, L., 2013. Evapotranspiration measurement and estimation using modified Priestley–Taylor model in an irrigated maize field with mulching. *J. Agric. Forest Meteorol.* 168, 140–148.
- Dyer, A.J., Crawford, T.V., 1965. Observations of the modification of the microclimate at a leading edge. *Quart. J. Royal Meteor. Soc.* 91, 345–348.
- Huntington, J., Szilagyi, J., Tyler, S., Pohl, G., 2011. Evaluating the complementary relationship for estimating evapotranspiration from arid shrublands. *Water Resour. Res.* 47, W05533.
- Jiang, L., Islam, S., 2001. Estimation of surface evaporation map over Southern Great Plains using remote sensing data. *Water Resour. Res.* 37 (2), 329–340.
- Kim, S., Kim, H.S., 2008. Neural networks and genetic algorithm approach for nonlinear evaporation and evapotranspiration modeling. *J. Hydrol.* 351 (3–4), 299–317.
- Klein, J., 2013. Water Resource Sensitivity from a Mediterranean Perspective: Using a Hydrological model to Explore the Combined Impacts of Climate and Land-Water Management Changes. MS Thesis, Department of Physical Geography and Quaternary Geology, Stockholm University, Sweden.
- Kustas, W., Anderson, M., 2009. Advances in thermal infrared remote sensing for land surface modeling. *Agric. Forest Meteorol.* 149 (12), 2071–2081.
- Lobell, D.B., Bonfils, C., 2008. The effect of irrigation on regional temperatures: a spatial and temporal analysis of trends in California, 1934–2002. *J. Climate* 21 (9), 2063–2071.
- McMahon, T.A., Peel, M.C., Lowe, L., Srikanthan, R., McVicar, T.R., 2013. Estimating actual, potential, reference crop and pan evaporation using standard meteorological data: a pragmatic synthesis. *Hydrol. Earth System Sci.* 17, 1331–1363.
- Monteith, J.L., 1965. Evaporation and environment. In: *Proceedings of the 19th Symposium of the Society for Experimental Biology*. Cambridge University Press.
- Monteith, J.L., 1981. Evaporation and surface temperature. *Quart. J. Royal Meteor. Soc.* 107, 1–27.
- Morton, F.I., Ricard, F., Fogarasi, F., 1985. Operational Estimates of areal Evapotranspiration and Lake Evaporation – Program WREVAP. National Hydrologic Research Institute Paper No. 24. Ottawa, Canada.
- Nishida, K., Nemani, R.R., Running, S.W., Glassy, J.M., 2003. An operational remote sensing algorithm of land surface evaporation. *J. Geophys. Res.* 108 (D9), 4270.
- Ortman, C.L., 2009. Okavango River Basin Technical Diagnostic Analysis: Environmental Flow Modul Specialist Report. The Permanent Okavango River Basin Water Commission, Maun, Botswana.
- Penman, H.L., 1948. Natural evaporation from open water, bare soil, and grass. *Proc. Royal Soc. London A193*, 120–146.
- Philip, J.R., 1987. Advection, evaporation, and surface resistance. *Irrig. Sci.* 8, 101–114.
- Priestley, C.H.B., Taylor, R.J., 1972. On the assessment of surface heat flux and evaporation using large-scale parameters. *Month. Weather Rev.* 100 (2), 81–92.
- Rao, K.S., Wyngaard, J.C., Cote, O.R., 1974. Local advection of momentum, heat, and moisture in micrometeorology. *Boundary-Layer Meteorol.* 7, 331–348.
- Rider, N.E., Philip, J.R., Bradley, E.F., 1963. The horizontal transport of heat and moisture – a micrometeorological study. *Quart. J. Royal Meteor. Soc.* 89, 507–531.
- Sinkevich Jr., M.G., Walter, M.T., Lembo Jr., A.J., Richards, B.K., Peranginangin, N., Aburime, S.A., Steenhuis, T.S., 2005. A GIS-based groundwater contamination risk assessment tool for pesticides. *Groundwater Monitor. Remed.* 25 (4), 82–91.
- Souch, C., Wolfe, C.P., Grimmond, C.S.B., 1996. Wetland evaporation and energy partitioning: Indiana Dunes National Lakeshore. *J. Hydrol.* 184, 189–208.
- Spittlehouse, D.L., Black, T.A., 1981. A growing season water balance model applied to two Douglas fir stands. *Water Resour. Res.* 17, 1651–1656.
- Szilagyi, J., 2013a. Application of MODIS-based monthly evapotranspiration rates in runoff modeling: a case study in Nebraska, USA. *Open J. Modern Hydrol.* 3, 172–178.
- Szilagyi, J., 2013b. Recent Updates of the Calibration-free Evapotranspiration Mapping (CREMAP) Method. In: Alexandris, S.G. (ed.) *Evapotranspiration – An Overview*, InTech, Rijeka, Croatia, open access at <<http://www.intechopen.com/books/evapotranspiration-an-overview>>
- Szilagyi, J., Jozsa, J., 2008. New findings about the complementary relationship-based evaporation estimation methods. *J. Hydrol.* 354 (1–4), 171–186.
- Szilagyi, J., Kovacs, A., 2010. Complementary-relationship-based evapotranspiration mapping (CREMAP) technique for Hungary. *Period. Polytech. – Civil Eng.* 54 (2), 95–100.
- Szilagyi, J., Schepers, A., 2014. Coupled heat and vapor transport: the thermostat effect of a freely evaporating land surface. *Geophys. Res. Lett.* 41. <http://dx.doi.org/10.1002/2013GL058979>.
- Szilagyi, J., Hobbins, M.T., Jozsa, J., 2009. Modified advection-aridity model of evapotranspiration. *J. Hydrol. Eng.* 14 (6), 569–573.
- Szilagyi, J., Kovacs, A., Jozsa, J., 2011. A calibration-free evapotranspiration mapping (CREMAP) technique. In: Labeledzki, L. (Ed.) *Evapotranspiration*, InTech, Rijeka, Croatia, open access at <<http://www.intechweb.org/books/show/title/evapotranspiration>>

- Taylor, P.A., 1971. Airflow above changes in surface heat flux, temperature and roughness; an extension to include the stable case. *Boundary-Layer Meteorol.* 1, 474–497.
- Thornthwaite, C.W., Mather, J.R., 1955. *The Water Balance*. Drexel Institute of Technology Climatological Laboratory Publication #8.
- Wang, K., Dickinson, R.E., 2012. A review of global terrestrial evapotranspiration: observation, modeling, climatology, and climatic variability. *Rev. Geophys.* 50, 1–54, RG2005.
- Wang, K., Li, Z.Q., Cribb, M., 2006. Estimation of evaporative fraction from a combination of day and night land surface temperatures and NDVI: a new method to determine the Priestley–Taylor parameter. *Remote Sens. Environ.* 102 (3–4), 293–305.
- Wolski, P., Murray-Hudson, M., 2005. Modelling of the effects of various water abstraction patterns on the ecology of the flood-pulsed Okavango-Delta, Botswana. W3M conference, Wierzba, Poland.